

Article

Association of Keplerate-Type Polyoxometalate {Mo₇₂Fe₃₀} with Tetracycline: Nature of Binding Sites and Antimicrobial Action

Kirill Grzhegorzhevskii ^{1,*}, Margarita Tonkushina ¹, Pavel Gushchin ¹, Ilya Gagarin ¹, Alexander Ermoshin ¹, Kseniya Belova ¹, Anna Prokofyeva ¹, Alexander Ostroushko ¹ and Alexander Novikov ²

¹ Institute of Natural Sciences and Mathematics, Ural Federal University, Mira St. 19, 620002 Ekaterinburg, Russia

² Institute of Chemistry, Saint Petersburg State University, Universitetskaya Nab. 7/9, 199034 Saint Petersburg, Russia

* Correspondence: kirillvalentinovich@urfu.ru

Abstract: The association process between the tetracycline (TC) antibiotic molecule and Keplerate-type nanocluster polyoxometalate (POM) {Mo₇₂Fe₃₀} was studied in aqueous solution. The novel supramolecular ensemble {Mo₇₂Fe₃₀}@TC_{12.5} was produced, its composition and structure were revealed by means of elemental analysis (C, N, H) and vibrational spectroscopy (IR and Raman). Based on the spectral data, the POM structure's integrity was confirmed and binding sites of TC with the Keplerate {Mo₇₂Fe₃₀} surface were found. Due to thermogravimetric analysis (TG) and in-situ Raman spectroscopy during the process of {Mo₇₂Fe₃₀}@TC_{12.5} thermal destruction, we showed a significant change in the phase composition of POM's destruction products after association with TC. The antibacterial activity of the obtained complex {Mo₇₂Fe₃₀}@TC_{12.5} was examined. The experimental results allowed us to note the partial inhibition of TC's antibacterial activity owing to the coordination of TC to Fe^{III} centers, in turn, which hinders the participation of TC in coordination via Mg²⁺ of ribosomal subunits 30S in bacteria.

Keywords: polyoxometalate; tetracycline; Keplerate; vibrational spectroscopy; antibiotic action



Citation: Grzhegorzhevskii, K.; Tonkushina, M.; Gushchin, P.; Gagarin, I.; Ermoshin, A.; Belova, K.; Prokofyeva, A.; Ostroushko, A.; Novikov, A. Association of Keplerate-Type Polyoxometalate {Mo₇₂Fe₃₀} with Tetracycline: Nature of Binding Sites and Antimicrobial Action. *Inorganics* **2023**, *11*, 9. <https://doi.org/10.3390/inorganics11010009>

Academic Editor: Claudio Pettinari

Received: 7 December 2022

Revised: 21 December 2022

Accepted: 21 December 2022

Published: 25 December 2022



Copyright: © 2022 by the authors. Licensee MDPI, Basel, Switzerland. This article is an open access article distributed under the terms and conditions of the Creative Commons Attribution (CC BY) license (<https://creativecommons.org/licenses/by/4.0/>).

1. Introduction

The chemistry of giant nanocluster polyoxometalates (POM), particularly with toroidal ({Mo₁₅₄}) and Keplerates ({Mo₁₃₂}, {Mo₇₂Fe₃₀}) structures, has a great potential in the functional design of supramolecular structures including template effects. The POMs' sizes are in the range of 2.5 nm to 3.6 nm [1–3], and their hydrophilic surface could be modified using electrostatic and van der Waals's forces, hydrogen bonding (with non-ionic polymers [4]) and coordination interaction (NO₂ absorption by {Mo₇₂Fe₃₀} crystals [5]). Furthermore, recently, the possibility of the covalent modification of Keplerates {Mo₁₃₂} and {Mo₇₂Fe₃₀} by alkoxysilane molecules was shown [6]. Electrostatic bonding is one of the simplest ways to obtain strong POM's associates with different types of cations: photosensitizers (rhodamine B, ΔG_{bond} with {Mo₁₃₂} is −37.4 kJ·mol^{−1} [7], where intermolecular charge transfer and dye J-aggregates formation take place), bioactive substances (for example vitamin B1, ΔG_{bond} with {Mo₇₂Fe₃₀} is −570.8 J·g^{−1} [8,9]) and multicharged metal ions (Cd⁺³ [10]). In this context, it should be noted that the Keplerate {Mo₇₂Fe₃₀}=[Mo₇₂Fe₃₀O₂₅₂(CH₃COO)₁₂{Mo₂O₇(H₂O)}₂{H₂Mo₂O₈(H₂O)}(H₂O)₉₁].150H₂O is non-toxic in vitro because of a lack of Mo(V), the presence of which provides a redox reaction [11]. Thus, this Keplerate could be used as a nano core for drug binding [12]. Such binding opens up additional pathways for drug delivery, for example, via iontophoresis [12,13]. Moreover, the Keplerate {Mo₇₂Fe₃₀} is able to induce cellular endocytosis, expanding the cellular membrane surface [14,15]. In general, the concept of supramolecular template synthesis suggests that POMs, in particular {Mo₇₂Fe₃₀}, can act as templates for

the forming of a multicomponent shell. These shells can consist of drugs, fluorescent labels, protective molecules and molecular vectors. They can help to prevent the competitive binding to blood proteins and for the targeting of these supramolecular ensembles to the tissues of the body.

The binding of POM with antibiotics, as one of the most important classes of drugs, can find application in biotechnology. POMs and antibiotics associates can serve several goals: increasing penetrating ability, decreasing antibiotic resistance of some strains, and increasing therapy targeting due to conjugation with vector molecules of various natures via shared POM particles serving as a nano-core.

In this work, we study an interaction between a tetracycline (TC) antibiotic and Keplerate $\{\text{Mo}_{72}\text{Fe}_{30}\}$ (Figure 1). The molecular scaffold, consisting of four conjugated rings with alternating hydroxyl and carbonyl groups, underlying the structure of tetracycline is an important building block for drug design. TC exhibits complexing ability towards metal ions, particularly lanthanides Ln(III) [16] and iron [17], due to a chelating effect. The antibacterial activity of TC occurs via the magnesium ion Mg^{2+} chelating of, and subsequent binding to, the phosphate groups in the 30S ribosomal subunit [18]. Thus, study of the association of TC with Keplerate $\{\text{Mo}_{72}\text{Fe}_{30}\}$ helps to combine different approaches to create functionalized nanoscaled ensembles with antibacterial effect. Indeed, the interaction between the TC and $\{\text{Mo}_{72}\text{Fe}_{30}\}$ surface occurs both due to electrostatic interactions between the protonated tertiary nitrogen atom in the TC and the $\{\text{Fe-OH}^-\}$ vertex in the iron polyhedron (which dissociates in an acidic manner from the maximum negative charge of POM in water, -22 [19]), and due to the coordination of the TC with the iron atom. In addition, one cannot exclude the presence of the chaotropic effect, which was recently found and comprehensively studied for aqueous solutions of POMs, cyclodextrins [20–23] and nonionic surfactants [24]. Based on the possibility of the chelation of Fe(III) ions in $\{\text{Mo}_{72}\text{Fe}_{30}\}$ by TC molecules, it cannot be ruled out that this can lead to the destruction of the Keplerate or rearrangement of its structure, which is typical for giant Keplerate POMs [3,25].

Thus, the study of the TC association with iron-molybdenum POM is relevant not only from the point of view of bio-application, but also structural coordination chemistry. In this work, the complex $\{\text{Mo}_{72}\text{Fe}_{30}\}@TC$ was obtained for the first time and the composition and structure were determined using elemental C, N, H analysis and vibrational IR and Raman spectroscopy. Due to the high symmetry point group I_h of $\{\text{Mo}_{72}\text{Fe}_{30}\}$, the vibrational spectra turn out to be very sensitive to the structural integrity of this POM, which was shown earlier in the course of a comprehensive study of several nanoclusters from the giant POM family [26]. The use of IR and Raman spectroscopy showed the preservation of the nanocluster's structure upon interaction with TC and made it possible to establish the nature of the binding centers. In addition, we estimated the antibacterial effect of the associate $\{\text{Mo}_{72}\text{Fe}_{30}\}@TC$ in relation to the strains of *Escherichia coli* (HB101, JM110 and TOP10) in comparison with the POM, its degradation products, and simple iron and molybdenum salts in equivalent concentrations.

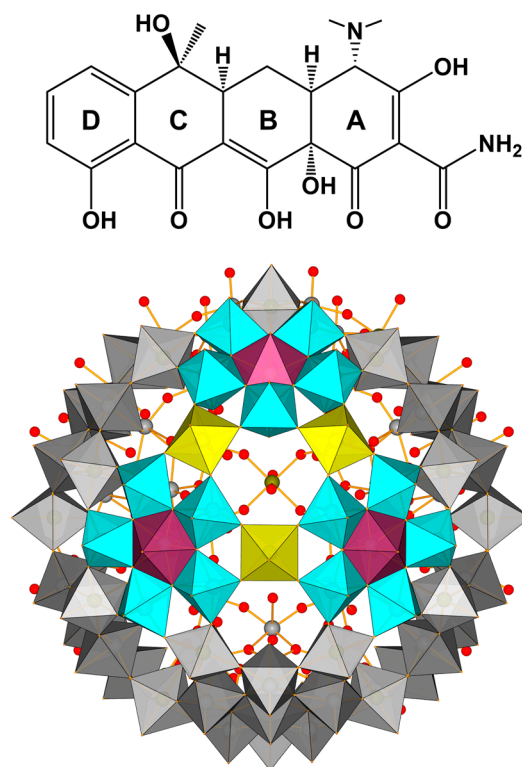


Figure 1. The structure of tetracycline (TC) and Keplerate $\{Mo_{72}Fe_{30}\}$, represented by the frontal part in the form of molybdenum (VI) and iron (III) oxygen polyhedra. Polyhedra code: yellow— FeO_6 ; light blue— MoO_6 ; purple— MoO_7 . Atomic code: yellow—iron; gray—molybdenum; red—oxygen.

2. Results and Discussion

In order to determine the complex stoichiometry, we prepared two samples with POM:TC ratio as 1:10 and 1:20 in aqueous solution. During the mixing of these components the dark-brown amorphous precipitate appeared wherein the deposition rate is higher with more TC concentration. The produced samples $\{Mo_{72}Fe_{30}\}@TC_x$ were dried at room temperature and used for elemental analysis, which showed the mass fraction (mass.%) values for POM:TC=1:10 the content of Mo, C, N, H: 38.13, 17.31, 1.68, 2.82% and for POM:TC=1:20 the content of Mo, C, N, H: 33.875, 19.50, 1.91, 3.07%. Based on these data, we found the structural formulas as $[Mo_{72}Fe_{30}O_{252}(CH_3COO)_{10}(C_{22}H_{24}N_2O_8)_{11}(H_2O)_{91}(H_2O)'_{15}]$ for POM:TC=1:10 and $[Mo_{72}Fe_{30}O_{252}(CH_3COO)_{11}(C_{22}H_{24}N_2O_8)_{14}(H_2O)_{91}(H_2O)'_{15}] \cdot 20H_2O$ for the POM:TC=1:20 molar ratio. Averaging on the tetracycline and acetate groups content, we obtained $\{Mo_{72}Fe_{30}\}@TC_{12.5}=[Mo_{72}Fe_{30}O_{252}(CH_3COO)_{10.5}(C_{22}H_{24}N_2O_8)_{12.5}(H_2O)_{91}(H_2O)'_{15}] \cdot (20-x)H_2O$, where x is from 0 to 20. However, the question about constitution and cluster water content had not yet been answered. Further TG measurements indicated for initial $\{Mo_{72}Fe_{30}\}$ that mass loss (14%) finished at 220 °C, which corresponds to the first stage of the dehydration process [27]. For $\{Mo_{72}Fe_{30}\}@TC_{12.5}$, the mass loss is 8.2% at this temperature (vide infra), whereas, for associates $\{Mo_{72}Fe_{30}\}@TC_{11}$ and $\{Mo_{72}Fe_{30}\}@TC_{14}$ containing 106 and 126 H_2O molecules, respectively, theoretical values are 9.5 and 10.4%, respectively. Taking into account the accuracy of TG measurements, the experimental and calculated data are in agreement.

From a structural point of view, to interpret the elemental analysis one should pay attention to the specificity of the $\{Mo_{72}Fe_{30}\}$ structure (Figure 1). Iron-molybdenum POM consists of 30 Fe^{III} octahedra and 12 $\{Mo^{VI}_6\}$ blocks. In turn, the latter is built from pentagonal bipyramid connected with five $\{Mo^{VI}_6\}$ octahedra in the equatorial plane. For each block $\{Mo_6\}$, there are 15 oxygen atoms in the equatorial plane, 6 oxygen vertices toward the outer shell and 6 toward the inner part—into the POM cavity. Equatorial and outer shell oxygen atoms ($21 \times 12 = 252$) are not protonated, whereas terminal inner

oxygen atoms in $\{\text{Mo}_6\}$ and both up and down vertices in $\{\text{FeO}_6\}$ polyhedra are represented by aqualigands (91 H_2O) and acetate groups (12 CH_3COO^- per POM); if we calculate, we have $6 \times 12 + 2 \times 30 = 132$ oxygen vertices. Aqualigands (91) and bidentate acetate groups (12) relate only to 115 oxygen vertices. The residual 17 down vertices correspond to bridge-oxygen atoms in $\{\text{Mo}_2\text{O}_7(\text{H}_2\text{O})\}_2\{\text{H}_2\text{Mo}_2\text{O}_8(\text{H}_2\text{O})\}$ located in the inner POM cavity [3]. As a result of molecules' coordination with the $\{\text{Mo}_{72}\text{Fe}_{30}\}$ surface, the release of this inner cavity fragment occurs [28]; therefore, the 17 oxygen vertices remain vacant and have to be occupied with either aqualigands or acetate groups, or oxygen atoms from guest molecules.

In the case of associates produced at the POM:TC=1:10 ratio, the structural formula $[\text{Mo}_{72}\text{Fe}_{30}\text{O}_{252}(\text{CH}_3\text{COO})_{10}(\text{C}_{22}\text{H}_{24}\text{N}_2\text{O}_8)_{11}(\text{H}_2\text{O})_{91}(\text{H}_2\text{O})'_{15}]$ suggests that water molecules and acetate groups can occupy 126 oxygen vertices only, whereas 6 vertices remain vacant. Worth noting is that interaction between TC and POM leads to stoichiometric complex formation even under a lack of TC (extra POM remain free in solution); we can suppose that some of the vacant oxygen vertices are occupied with oxygen from TC. Under a 20-fold molar excess of TC, the precipitate contains an additional 20 water molecules, which is enough to completely saturate the coordination sphere of iron and molybdenum in polyhedra. However, in accordance with how TC coordinates with POM surface (vide infra), it seems logical to assume that at least one oxygen atom of each TC is coordinated to the metal center (iron center, which has a great affinity with TC [17]). Consequently, in the associate structure, a number of the water molecules should be transferred to the second coordination sphere: $[\text{Mo}_{72}\text{Fe}_{30}\text{O}_{252}(\text{CH}_3\text{COO})_{10.5}(\text{C}_{22}\text{H}_{24}\text{N}_2\text{O}_8)_{12.5}(\text{H}_2\text{O})_{91}(\text{H}_2\text{O})'_{9}] \cdot (\text{H}_2\text{O})'_6 \cdot (20-x)\text{H}_2\text{O}$, where the x is from 0 to 20.

The coordination nature and localization of binding centers in TC molecules bound to POM were studied with IR and Raman spectroscopy (Figures 2 and 3). Below 1000 cm^{-1} (Figure 2), IR spectrum showed the presence of all characteristic bands for $\{\text{Mo}_{72}\text{Fe}_{30}\}$ and, consequently, the preservation of the POM's structure during the associate formation with TC (in brackets, the value of the band position for pure $\{\text{Mo}_{72}\text{Fe}_{30}\}$ is given if it is different to the associate $\{\text{Mo}_{72}\text{Fe}_{30}\}@\text{(TC)}_{12.5}$): 968, 933 (947), 852 (850), 760 (756), 625 (631), 550 (553) cm^{-1} . Wherein, the stretchings of $\nu(\text{Fe-OH})$ at 1045 and 1032 cm^{-1} were not observed for associate $\{\text{Mo}_{72}\text{Fe}_{30}\}@\text{(TC)}_{12.5}$, but should appear for the initial POM [26]. Furthermore, low-energy shifts were registered for several bands: $\nu(\text{Mo=O})$ 947 \rightarrow 933 cm^{-1} , $\nu(\text{Mo}-\mu_2\text{O-Mo}/\text{Mo}-\mu_3\text{O-Mo})$ 631 \rightarrow 625 cm^{-1} and $\delta([\text{Mo}/\text{Fe}]-\text{O-Mo})$ 553 \rightarrow 550 cm^{-1} , whereas for the other bands high-energy shifts occurred: $\nu([\text{Mo}/\text{Fe}]-\text{O-Mo})$ 756 \rightarrow 760 cm^{-1} and $\nu(\text{Mo-O-Mo}/\text{O-Mo-O})$ 850 \rightarrow 852 cm^{-1} . Both the low-energy shift (by 14 cm^{-1}) for terminal group $\nu(\text{Mo=O})$ and the disappearing of the Fe-OH signal correspond to the strong participation of these surface centers in the interaction with TC. In addition, such interaction indirectly influences the normal mode frequencies related with bridging iron and molybdenum atoms. In particular, high-energy shifts are conditioned with a bond force constant increase (in the harmonic oscillator model), which reflects the rearranging of electron density in the POM structure, revealing the strong interaction between TC and the POM's surface.

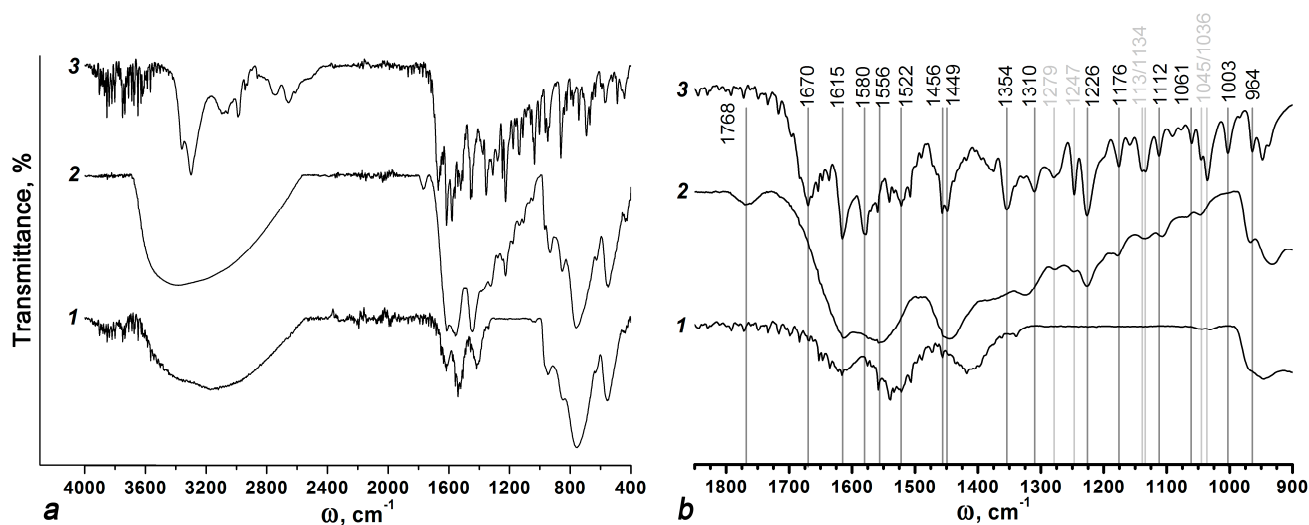


Figure 2. IR-spectra (ATR mode) of $\{Mo_{72}Fe_{30}\}$, $\{Mo_{72}Fe_{30}\}@TC_{12.5}$ and $TC \cdot HCl$ (from bottom to top 1, 2, 3, respectively) in the full spectral range (a) and in the specific range (b).

In line with $TC \cdot HCl$ structure, we expected electrostatic bonding between the protonated tertiary nitrogen atom in TC and the weak acid center $Fe-OH_2 \leftrightarrow FeOH^- + H^+$. In accordance with IR data, TC–POM interaction led to the significant broadening of the I-amide band (1670 cm^{-1} , $\nu(C=O)$), which practically disappeared. The II-amide band (1522 cm^{-1} , $\delta(NH_2)$ [29]) also underwent a large broadening and shifted to 1556 cm^{-1} . The observed shift is not due to overlapping with the $\nu_{as/s}$ stretching of the acetate group in POM (1532 and 1411 cm^{-1}), which is proved by the mutual decrease in these vibrations after $\{Mo_{72}Fe_{30}\}$ association with TC. The stretching of carbonyl group $\nu(C=O)$ in the A-ring at 1615 cm^{-1} maintains the original frequency, whereas the $C=O$ group in the C-ring [29] contributes to the interaction with POM, leading to the disappearance of corresponding vibrations at 1580 cm^{-1} . The presence of $C=O$ stretching in the C-ring at such a low wavenumber is caused by the participation of oxygen atoms in tautomeric equilibria with two protons of neighboring hydroxyl groups. This behavior is common for anthraquinone structures [30]. The involvement of one of the neighboring OH groups in binding to the POM leads to the disappearance of the tautomeric equilibrium and the liberation of the $C=O$ group [30]. This behavior is observed for IR spectrum of $\{Mo_{72}Fe_{30}\}@TC_{12.5}$, where the novel band of an unbound carbonyl group $C=O$ appears at 1768 cm^{-1} due to TC interaction with POM [31]. It is difficult to assign the remaining bands in the TC's spectrum due to the contribution of multiple functional groups to the normal vibrations with close frequencies. However, the analysis of bands' positions and relative intensities demonstrated that the characteristic band sets of TC stay practically unchanged, providing the preservation of the TC structure.

Investigation of associate $\{Mo_{72}Fe_{30}\}@TC_{12.5}$ by Raman spectroscopy showed the significant decrease in thermal stability. To perform the Raman measurement of pure POM, very low laser intensity and long acquisition time were used to prevent thermal destruction, in-situ, in the laser beam [26]. However, in contrast to initial Keplerate $\{Mo_{72}Fe_{30}\}$, we could not register the POM's spectral fingerprints when measuring the associate's spectrum because this measurement resulted in the thermal destruction of the whole system with the formation of $Fe_2(MoO_4)_3$ and $\alpha-MoO_3$. It is worth noting that during $\{Mo_{72}Fe_{30}\}$ destruction in the laser beam, the iron molybdate dominates the Raman spectrum because the main fraction of molybdenum from POM structure is spent on this phase formation, in accordance with $Fe_2(MoO_4)_3$ stoichiometry (Figure 3b) [26]. The found discrepancy in associate thermal destruction as compared to the destruction of individual components (TC and POM) are clearly shown in TG curves (Figure 3c) [32]. Along with spectral features corresponding to TC binding to POM, one can conclude that not only do simple electrostatic interaction occur but also the coordination of TC's functional group to iron centers in the

$\{\text{Mo}_{72}\text{Fe}_{30}\}$ structure. The latter leads to a decrease in the thermal stability and reduction in the iron molybdate fraction in destruction products.

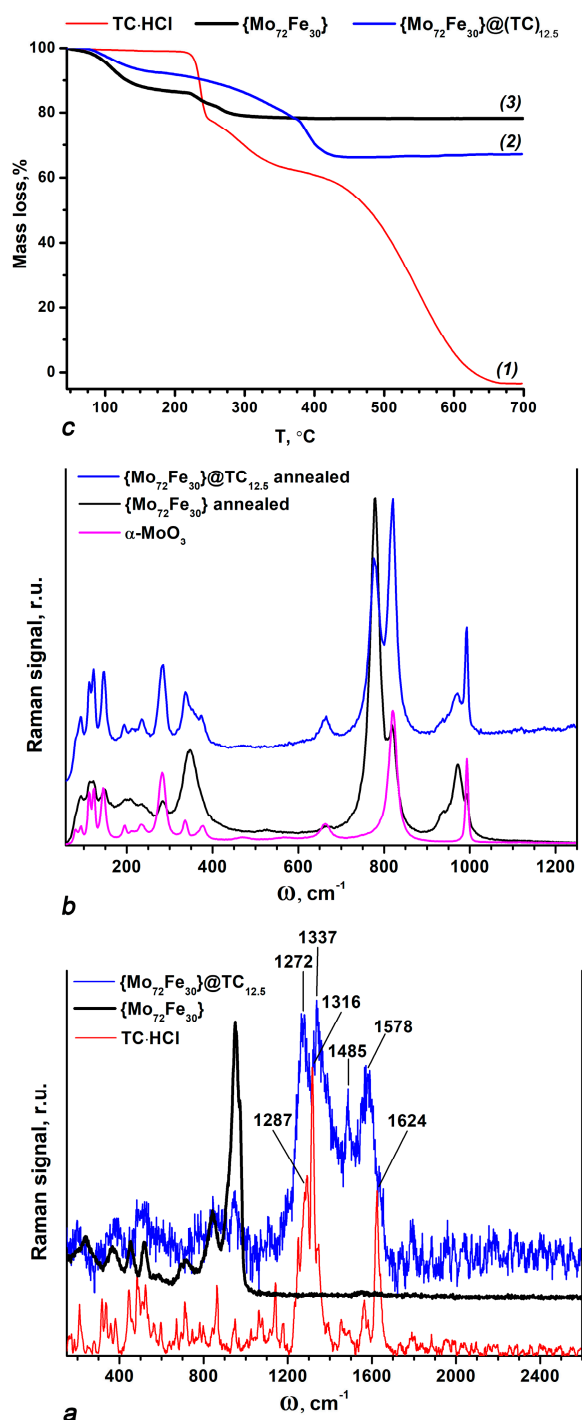


Figure 3. (a) Raman spectra (He–Ne laser with excitation wavelength 633 nm) of TC, $\{\text{Mo}_{72}\text{Fe}_{30}\}$ and $\{\text{Mo}_{72}\text{Fe}_{30}\}@TC_{12.5}$ (from bottom to top, respectively); (b) Raman spectra of $\alpha\text{-MoO}_3$, $\{\text{Mo}_{72}\text{Fe}_{30}\}$ thermal destruction products and $\{\text{Mo}_{72}\text{Fe}_{30}\}@TC_{12.5}$ destruction products in situ in the laser beam (from bottom to top, respectively); (c) TG curves of TC, $\{\text{Mo}_{72}\text{Fe}_{30}\}@TC_{12.5}$ and $\{\text{Mo}_{72}\text{Fe}_{30}\}$ (from bottom to top 1, 2, 3, respectively).

Focusing on the Raman spectrum of $\{\text{Mo}_{72}\text{Fe}_{30}\}@TC_{12.5}$ before thermal destruction, we can mention several features. After TC is coordinated with $\{\text{Mo}_{72}\text{Fe}_{30}\}$, the vibration of the vinyl fragment in the B-ring at 1624 cm^{-1} , related with hydroxyl group [33], practically

disappears from the spectrum. The coordination of this OH-group with the POM surface was monitored via IR spectra also (see supra). The carbonyl group stretching in the C-ring (with some contribution from skeleton C-C vibration in the D-ring), being normally at 1585 cm^{-1} for TC·HCl [33], shifted to 1578 cm^{-1} . The OH stretching in the D-ring and B-ring, which are neighbored with C=O (in C-ring), appears as a unified band at 1485 cm^{-1} , whereas for TC·HCl it is observed at 1453 cm^{-1} . Important is that the bending vibrations of methyl groups and NH on tertiary nitrogen atoms are revealed, for TC·HCl near this spectral region, at 1467 cm^{-1} [33]. Interestingly, $\nu(\text{C-O})$ stretching vibration in the D-ring appears at 1316 (intensive sharp peak) and 1347 cm^{-1} (middle signal) for TC·HCl, but after coordination to POM the first signal disappears whereas the second one shifts to 1337 cm^{-1} . The same shifting trend towards a low-frequency range is observed for $\delta(\text{CH}_2)$ and $\delta(\text{CH})$ bending vibrations in A-B-C-rings, which indirectly confirms the interaction of TC functional groups with the POM surface across these rings, wherein the D-ring slightly participates in such interactions.

Taking into account the spectral data and high TC affinity to the iron ions [17], as well as the coordination of guest molecules in $\{\text{Mo}_3\text{Fe}_3\text{O}_6\}$ pores (20 pores per POM) which is specific for Keplerate $\{\text{Mo}_{72}\text{Fe}_{30}\}$ [5,28], we made a 3D model of TC to POM coordination (Figure 4). In accordance with the electrostatic binding of protonated tertiary nitrogen atoms in TC with anion centers Fe-OH^- on the POM surface, as well as the coordination of the hydroxyl group in the B-ring and amide fragment, we placed TC molecule in the $\{\text{Mo}_3\text{Fe}_3\text{O}_6\}$ pore. Thus, the D-rings became naturally outlaying from the POM surface. For modelling, the TC and POM structures were created from monocystal X-ray data [3,34]. The distances between molybdenum/iron atoms of $\{\text{Mo}_3\text{Fe}_3\text{O}_6\}$ and the terminal oxygen and nitrogen atoms of TC molecules are presented in Table 1 (for comparison, Fe1-O_t bond length is 2.097 \AA). As one can see from these data, the supposed 3D model of interaction between POM and TC in pores is in-line with both the vibrational spectroscopy results and crystallography requirements for bond lengths.

Table 1. Proposed interatomic distances from the model of TC coordination with the $\{\text{Mo}_3\text{Fe}_3\text{O}_6\}$ pore.

$\{\text{Mo}_{72}\text{Fe}_{30}\}@TC_{12.5}$	Fe1-O1	(Fe2)O _t -N ⁺	Fe3-O _t	Fe3-O3	(Mo)O _t -H(amide)
	2.185 Å	2.194 Å	2.097 Å	2.589 Å	2.386–3.260 Å

Based on the found strong interaction between TC and POM surface, we studied how the coordination with Keplerate $\{\text{Mo}_{72}\text{Fe}_{30}\}$ influences the antimicrobial activity of tetracycline, which is important for the real application of such a system. The test experiment in a Petri dish containing agar media with a bacterial lawn of three strains of *E. coli* (HB101, JM110 and TOP10) was used to evaluate the antibacterial activity [35]. A total of $40\text{ }\mu\text{L}$ doses of the following examined solutions were placed into wells: TC; $\{\text{Mo}_{72}\text{Fe}_{30}\}$; sodium molybdate (Mo^{VI}); iron chloride hexahydrate (Fe^{III}); POM destruction products (DP); $\{\text{Mo}_{72}\text{Fe}_{30}\}@TC_{12.5}$; TC with sodium molybdate (TC+ Mo^{VI}); TC with iron chloride hexahydrate (TC+ Fe^{III}); and TC with DP (TC+DP). The Petri dish was incubated at $36\text{ }^\circ\text{C}$ overnight, then the diameters of sterile zones were determined (Figure 5). Obtained results are presented in Table 2.

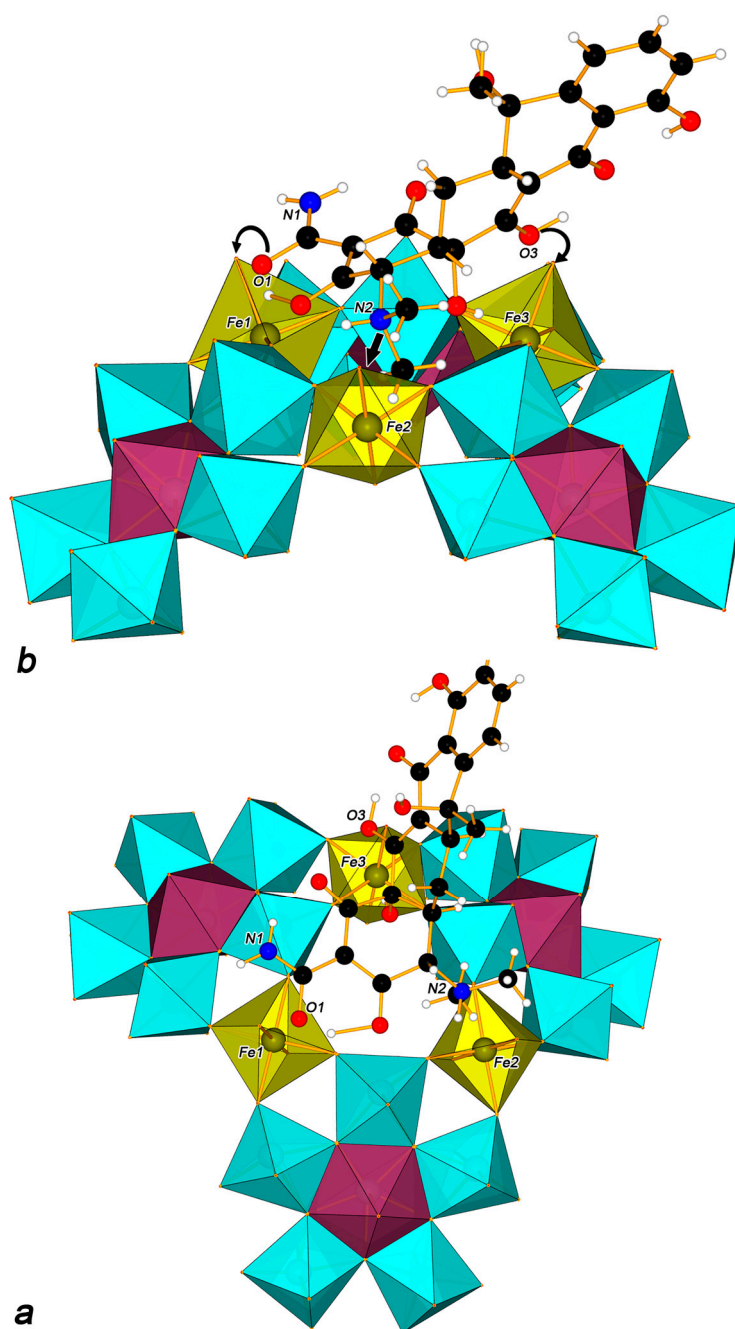


Figure 4. A 3D model of TC molecule binding to the $\{Mo_2Fe_3O_6\}$ pore in the $\{Mo_{72}Fe_{30}\}$ structure from various angles (a,b). Polyhedra code: yellow—FeO₆; light blue—MoO₆; purple—MoO₇. Atomic code: black—carbon; blue—nitrogen; red—oxygen.



Figure 5. Photo of a Petri dish with agar LB medium inoculated with *E. coli*, after the formation of sterile zones. There are solutions in the wells: 1— $\{\text{Mo}_{72}\text{Fe}_{30}\}$; 2—TC; 3— $\{\text{Mo}_{72}\text{Fe}_{30}\}$ @TC_{12.5}; 4— $\{\text{Mo}_{72}\text{Fe}_{30}\}$ destruction products (DP); 5—TC+DP; 6— $\text{FeCl}_3 \cdot 6\text{H}_2\text{O}$; 7—TC+ $\text{FeCl}_3 \cdot 6\text{H}_2\text{O}$; 8— $\text{Na}_2\text{MoO}_4 \cdot 2\text{H}_2\text{O}$; 9—TC+ $\text{Na}_2\text{MoO}_4 \cdot 2\text{H}_2\text{O}$.

Table 2. The antimicrobial activity towards *E. coli* strains.

Strain	Average Diameters of Sterile Zones (mm) for <i>E. coli</i> Strains								
	TC	$\{\text{Mo}_{72}\text{Fe}_{30}\}$	Mo^{VI}	Fe^{III}	DP	$\{\text{Mo}_{72}\text{Fe}_{30}\}$ @TC _{12.5}	TC+ Mo^{VI}	TC+ Fe^{III}	TC+DP
HB101	8.3 ± 0.5	0.0	0.0	0.0	0.0	6.3 ± 0.5	7.3 ± 0.4	6.0 ± 0.4	6.2 ± 1.2
JM110	7.7 ± 0.8	0.0	0.0	0.0	0.0	6.2 ± 0.8	7.5 ± 0.0	7.7 ± 0.7	4.8 ± 0.2
TOP10	6.7 ± 0.4	0.0	0.0	0.0	0.0	5.2 ± 0.2	5.5 ± 0.0	6.0 ± 0.0	6.2 ± 1.1

Reliability analysis of obtained data was performed by means of the nonparametric Mann–Whitney U test which showed that neither initial POM $\{\text{Mo}_{72}\text{Fe}_{30}\}$ nor its destruction products nor iron nor molybdenum salts possess evident antimicrobial activity in used concentrations. Furthermore, the antimicrobial activity of TC is significantly decreased after interaction with either $\{\text{Mo}_{72}\text{Fe}_{30}\}$, DP or iron salt. In the case of iron molybdate, the statistically significant decrease in TC activity was observed for the strain TOP10 only. Therefore, in both POM structure and simple low-molecular weight substances, the coordination with Fe^{III} centers is related to the partial suppression of TC antimicrobial activity. Probably, complexation with iron hinders the effective TC coordination with Mg^{2+} ions in bacterial cells, which is needed for TC coordination to ribosomal subunit 30S to suppress the protein synthesis, in turn [18]. The effect found here indirectly confirms the specific TC coordination to iron centers in the $\{\text{Mo}_{72}\text{Fe}_{30}\}$ @TC_{12.5} structure, which can be used for the local inhibition of TC activity.

3. Materials and Methods

Keplerate-type polyoxometalate $\{\text{Mo}_{72}\text{Fe}_{30}\}$ was produced in accordance with established procedures [3] by substitution of a Mo^{V} in ammonium salt $(\text{NH}_4)\{\text{Mo}_{132}\}$ with Fe^{III} ; all reagents were of analytical grade and were used without further purification. $(\text{NH}_4)\{\text{Mo}_{132}\}$ was synthesized in accordance with established procedures [2].

The structures of $(\text{NH}_4)\{\text{Mo}_{132}\}$ and $\{\text{Mo}_{72}\text{Fe}_{30}\}$ were confirmed by comparison of FTIR and Raman spectra with reference data [2,3,26]. Experimental IR bands for $\{\text{Mo}_{72}\text{Fe}_{30}\}$: $\sim 3340\text{s}$, $\sim 3165\text{s}$, $\sim 3030\text{m}$, 1613m , 1532s , 1411s , 1342w , 1045w , 1032w , $965\text{s}/945\text{s}$, 849s , 749vs , 624m , 547s , 435w ; Raman bands: 969s (sh), 952vs , 909m (sh), 842m , 717m , 586vw , 518m , 452m , 370m , 240m . Experimental IR bands for $(\text{NH}_4)\{\text{Mo}_{132}\}$: 3470s , 3215s , $3050\text{s}/2855\text{m}$, 1711w , 1614m , 1549s , 1418s , 1350w (sh), 1337w , $1105\text{vw}/1050\text{vw}$, 968s , $938\text{s}/854\text{m}$, 795s , 724s , 634m , 573m , 512m , 472m , 451w , 439w , 419w ; Raman bands: 1250w (comb.), 945m , 875s , 842m (sh), 715w (comb.), 376s , 316m , 215w .

The synthesis of the $\{\text{Mo}_{72}\text{Fe}_{30}\}@\text{(TC)}_x$ associate was carried out by dropwise addition of TC·HCl (tetracycline hydrochloride, Sigma-Aldrich, 95%) 4×10^{-2} M aqueous solution to $\{\text{Mo}_{72}\text{Fe}_{30}\}$ aqueous solutions 1×10^{-4} M while stirring, the molar ratio of the components in the final mixtures was POM:TC = 1:10 and 1:20. The amorphous precipitate was collected after 24 h by centrifugation of the mixture at 6000 rpm for 10 min. The resulting precipitate was mixed with 12 mL of distilled water on a vortex (2700 rpm, 10 min) and centrifuged (6000 rpm, 10 min), the liquid phase was then removed. This washing cycle was repeated three times; the precipitate purified from the free TC was dried at 40°C under vacuum. The resulting powder was the $\{\text{Mo}_{72}\text{Fe}_{30}\}@\text{(TC)}_x$ associate.

Elemental analysis was performed with automatic element analyzer CHNS PE 2400, series II (Perkin Elmer Instruments, USA). The IR spectra were recorded using FT-IR spectrometer Nicolet 6700 (Thermo Scientific, USA) in ATR mode. The Raman spectra were obtained using the confocal Raman microscope Alpha 300 AR (WiTec GmbH, Germany) with low-power laser beam (He–Ne laser with excitation wavelength 633 nm) in order to prevent the uncontrollable destruction of the samples [26].

Thermal gravimetric analysis was carried out with thermoanalyser STA 409 Luxx (Netzsch, Germany) under air atmosphere; the samples were heated from 45 to 700°C at a rate of 10°C per minute.

Antibacterial activity against *E. coli* strains (HB101, JM110 and TOR 10) was determined by the following method [35]. A total of 20 mL of agar LB medium was added to Petri dishes (diameter 9 cm) and *E. coli* cultures were inoculated. In addition, $40\ \mu\text{L}$ aliquots of the studied solutions were placed into wells made in the medium. The concentration of tetracycline was $0.2\ \text{g/L}$, the concentration of POM was $0.65\ \text{g/L}$ (which corresponded to the molar ratio of TC:POM = 12:1), the concentrations of iron chloride and sodium molybdate corresponded to the iron and molybdenum content of the samples with POM. Petri dishes were incubated overnight at 36°C . Then, the diameter of the sterile zone was determined in 2 analytical (measurements in two perpendicular directions of one sample) and 3 biological (3 separate Petri dishes) repetitions.

4. Conclusions

It can be concluded that we obtained a novel complex $\{\text{Mo}_{72}\text{Fe}_{30}\}@\text{TC}_{12.5}$ by the association of POM with tetracycline molecules in an aqueous solution. Based on the data of vibrational IR and Raman spectroscopy, it was found that the POM retains the integrity of its structure when interacting with the TC; in addition, the binding centers of the TC molecule on the POM's surface were determined and a 3D model of such an interaction was proposed, assuming the binding of the TC in the $\{\text{Mo}_3\text{Fe}_3\text{O}_6\}$ pore. Such binding occurs through: Coulomb interaction between the tertiary nitrogen atom in the NH^+ group and the $\text{Fe-OH}_2 \leftrightarrow \text{Fe-OH}^- + \text{H}^+$ acidic sites; through the amide group involved in the formation of hydrogen bonds with the oxygen vertices of the polyhedra in the POM's structure; and through the coordination of the hydroxyl group in B-ring to the Fe^{III} atom. At the same time, the D-ring of the TC molecule remains distant from the POM's surface and practically does not participate in the interaction. Such binding of TC to the POM's surface, as shown by TG and Raman spectroscopy, leads to a significant change in the nature of the thermal destruction of $\{\text{Mo}_{72}\text{Fe}_{30}\}@\text{TC}_{12.5}$ compared to its initial components. Taking into account the structural data on the $\{\text{Mo}_{72}\text{Fe}_{30}\}@\text{TC}_{12.5}$, an experiment was carried out to determine the effect of TC binding to POM on the antibacterial activity of TC. As a result,

the inhibition of the TC action by POM due to complex formation with Fe^{III} centers was shown. The obtained data on the {Mo₇₂Fe₃₀}-TC system can be used to design POM-based hybrid materials which have the function of releasing a variety bioactive molecules.

Author Contributions: Conceptualization, K.G., M.T. and A.O.; methodology, P.G., A.P., K.B. and A.E.; investigation, P.G., M.T., A.E., I.G. and K.G.; writing—original draft preparation, K.G., M.T., A.P., I.G.; writing—review and editing, A.N.; project administration, K.G. and A.N.; funding acquisition, K.G. All authors have read and agreed to the published version of the manuscript.

Funding: The research funding from the Ministry of Science and Higher Education of the Russian Federation (Ural Federal University Program of Development within the Priority-2030 Program) is gratefully acknowledged.

Institutional Review Board Statement: Not applicable.

Informed Consent Statement: Not applicable.

Data Availability Statement: Not applicable.

Conflicts of Interest: The authors declare no conflict of interest.

References

1. Müller, A.; Krickemeyer, E.; Meyer, J.; Bögge, H.; Peters, F.; Plass, W.; Diemann, E.; Dillinger, S.; Nonnenbruch, F.; Randerath, M.; et al. [Mo₁₅₄(NO)₁₄O₄₂₀(OH)₂₈(H₂O)₇₀]^{(25 ± 5)⁻: A Water-Soluble Big Wheel with More than 700 Atoms and a Relative Molecular Mass of About 24000. *Angew. Chem. Int. Ed. Engl.* **1995**, *34*, 2122–2124. [[CrossRef](#)]}
2. Müller, A.; Krickemeyer, E.; Bögge, H.; Schmidtman, M.; Peters, F. Organizational Forms of Matter: An Inorganic Super Fullerene and Keplerate Based on Molybdenum Oxide. *Angew. Chem. Int. Ed.* **1998**, *37*, 3359–3363. [[CrossRef](#)]
3. Müller, A.; Sarkar, S.; Shah, S.Q.N.; Bögge, H.; Schmidtman, M.; Sarkar, S.; Kögerler, P.; Hauptfleisch, B.; Trautwein, A.X.; Schünemann, V. Archimedean Synthesis and Magic Numbers: “Sizing” Giant Molybdenum-Oxide-Based Molecular Spheres of the Keplerate Type. *Angew. Chem. Int. Ed.* **1999**, *38*, 3238–3241. [[CrossRef](#)]
4. Ostroushko, A.A.; Safronov, A.P.; Tonkushina, M.O. Thermochemical Study of Interaction between Nanocluster Polyoxomolybdates and Polymers in Film Compositions. *Russ. J. Phys. Chem. A* **2014**, *88*, 295–300. [[CrossRef](#)]
5. Grzhegorzhevskii, K.V.; Tonkushina, M.O.; Fokin, A.V.; Belova, K.G.; Ostroushko, A.A. Coordinative Interaction between Nitrogen Oxides and Iron–Molybdenum POM Mo₇₂Fe₃₀. *Dalt. Trans.* **2019**, *48*, 6984–6996. [[CrossRef](#)]
6. Grzhegorzhevskii, K.V.; Denikaev, A.D.; Morozova, M.V.; Pryakhina, V.; Khairullina, E.; Tumkin, I.; Taniya, O.; Ostroushko, A.A. The Precise Modification of a Nanoscaled Keplerate-Type Polyoxometalate with NH₂-Groups: Reactive Sites, Mechanisms and Dye Conjugation. *Inorg. Chem. Front.* **2022**, *9*, 1541–1555. [[CrossRef](#)]
7. Fazylova, V.; Shevtsev, N.; Mikhailov, S.; Kim, G.; Ostroushko, A.; Grzhegorzhevskii, K. Fundamental Aspects of Xanthene Dye Aggregation on the Surfaces of Nanocluster Polyoxometalates: H- to J-Aggregate Switching. *Chem. A Eur. J.* **2020**, *26*, 5685–5693. [[CrossRef](#)]
8. Ostroushko, A.; Gagarin, I.; Tonkushina, M.; Grzhegorzhevskii, K.; Russkikh, O. Association of Spherical Porous Nanocluster Keplerate-Type Polyoxometalate Mo₇₂Fe₃₀ with Biologically Active Substances. *J. Clust. Sci.* **2018**, *29*, 111–120. [[CrossRef](#)]
9. Tonkushina, M.O.; Belozerova, K.A.; Gagarin, I.D.; Adamova, L.V.; Terziyan, T.V.; Russkikh, O.V.; Ostroushko, A.A. Thermodynamics of the Interaction between Keplerate-Type Polyoxometalate {Mo₇₂Fe₃₀} and Vitamin B1. *Thermochim. Acta* **2022**, *711*, 179201. [[CrossRef](#)]
10. Elistratova, J.; Akhmadeev, B.; Gubaidullin, A.; Korenev, V.; Sokolov, M.; Nizameev, I.; Stepanov, A.; Ismaev, I.; Kadirov, M.; Voloshina, A.; et al. Nanoscale Hydrophilic Colloids with High Relaxivity and Low Cytotoxicity Based on Gd(III) Complexes with Keplerate Polyanions. *New J. Chem.* **2017**, *41*, 5271–5275. [[CrossRef](#)]
11. Ostroushko, A.A.; Danilova, I.G.; Gette, I.F.; Medvedeva, S.Y.; Tonkushina, M.O.; Prokofieva, A.V.; Morozova, M.V. Study of Safety of Molybdenum and Iron-Molybdenum Nanocluster Polyoxometalates Intended for Targeted Delivery of Drugs. *J. Biomater. Nanobiotechnol.* **2011**, *2*, 557–560. [[CrossRef](#)]
12. Ostroushko, A.A.; Gagarin, I.D.; Grzhegorzhevskii, K.V.; Gette, I.F.; Vlasov, D.A.; Ermoshin, A.A.; Antosyuk, O.N.; Shikhova, S.V.; Danilova, I.G. The Physicochemical Properties and Influence on Living Organisms of Nanocluster Polyoxomolybdates as Prospective Bioinspired Substances (Based on Materials from the Plenary Lecture). *J. Mol. Liq.* **2020**, *301*, 110910. [[CrossRef](#)]
13. Ostroushko, A.A.; Gagarin, I.D.; Tonkushina, M.O.; Grzhegorzhevskii, K.V.; Danilova, I.G.; Gette, I.F.; Kim, G.A. Iontophoretic Transport of Associates Based on Porous Keplerate-Type Cluster Polyoxometalate Mo₇₂Fe₃₀ and Containing Biologically Active Substances. *Russ. J. Phys. Chem. A* **2017**, *91*, 1811–1815. [[CrossRef](#)]
14. Ostroushko, A.A.; Grzhegorzhevskii, K.V.; Medvedeva, S.Y.; Gette, I.F.; Tonkushina, M.O.; Gagarin, I.D.; Danilova, I.G. Physicochemical and Biochemical Properties of the Keplerate-Type Nanocluster Polyoxomolybdates as Promising Components for Biomedical Use. *Nanosyst. Phys. Chem. Math.* **2021**, *12*, 81–112. [[CrossRef](#)]

15. Ostroushko, A.A.; Ulitko, M.V.; Tonkushina, M.O.; Zubarev, I.V.; Medvedeva, S.Y.; Danilova, I.G.; Gubaeva, O.V.; Gagarin, I.D.; Gette, I.F. Influence of Nanocluster Molybdenum Polyoxometalates on the Morphofunctional State of Fibroblasts in Culture. *Nanotechnol. Russ.* **2018**, *13*, 1–10. [[CrossRef](#)]
16. Karthikeyan, G.; Mohanraj, K.; Elango, K.P.; Girishkumar, K. Synthesis, Spectroscopic Characterization and Antibacterial Activity of Lanthanide–Tetracycline Complexes. *Transit. Met. Chem.* **2004**, *29*, 86–90. [[CrossRef](#)]
17. Wang, H.; Yao, H.; Sun, P.; Li, D.; Huang, C.-H. Transformation of Tetracycline Antibiotics and Fe (II) and Fe (III) Species Induced by Their Complexation. *Environ. Sci. Technol.* **2016**, *50*, 145–153. [[CrossRef](#)]
18. Guerra, W.; Silva-Caldeira, P.P.; Terenzi, H.; Pereira-Maia, E.C. Impact of Metal Coordination on the Antibiotic and Non-Antibiotic Activities of Tetracycline-Based Drugs. *Coord. Chem. Rev.* **2016**, *327–328*, 188–199. [[CrossRef](#)]
19. Liu, T.; Imber, B.; Diemann, E.; Liu, G.; Cokleski, K.; Li, H.; Chen, Z.; Müller, A. Deprotonations and Charges of Well-Defined {Mo 72 Fe 30} Nanoacids Simply Stepwise Tuned by PH Allow Control/Variation of Related Self-Assembly Processes. *J. Am. Chem. Soc.* **2006**, *128*, 15914–15920. [[CrossRef](#)]
20. Izzet, G.; Ménand, M.; Matt, B.; Renaudineau, S.; Chamoreau, L.M.; Sollogoub, M.; Proust, A. Cyclodextrin-Induced Auto-Healing of Hybrid Polyoxometalates. *Angew. Chem. Int. Ed.* **2012**, *51*, 487–490. [[CrossRef](#)]
21. Assaf, K.I.; Ural, M.S.; Pan, F.; Georgiev, T.; Simova, S.; Rissanen, K.; Gabel, D.; Nau, W.M. Water Structure Recovery in Chaotropic Anion Recognition: High-Affinity Binding of Dodecaborate Clusters to γ -Cyclodextrin. *Angew. Chem. Int. Ed.* **2015**, *54*, 6852–6856. [[CrossRef](#)] [[PubMed](#)]
22. Falaise, C.; Khlifi, S.; Bauduin, P.; Schmid, P.; Shepard, W.; Ivanov, A.A.; Sokolov, M.N.; Shestopalov, M.A.; Abramov, P.A.; Cordier, S.; et al. “Host in Host” Supramolecular Core–Shell Type Systems Based on Giant Ring-Shaped Polyoxometalates. *Angew. Chem. Int. Ed.* **2021**, *60*, 14146–14153. [[CrossRef](#)] [[PubMed](#)]
23. Ivanov, A.A.; Falaise, C.; Shmakova, A.A.; Leclerc, N.; Cordier, S.; Molard, Y.; Mironov, Y.V.; Shestopalov, M.A.; Abramov, P.A.; Sokolov, M.N.; et al. Cyclodextrin-Assisted Hierarchical Aggregation of Dawson-Type Polyoxometalate in the Presence of {Re 6 Se 8} Based Clusters. *Inorg. Chem.* **2020**, *59*, 11396–11406. [[CrossRef](#)] [[PubMed](#)]
24. Naskar, B.; Diat, O.; Nardello-Rataj, V.; Bauduin, P. Nanometer-Size Polyoxometalate Anions Adsorb Strongly on Neutral Soft Surfaces. *J. Phys. Chem. C* **2015**, *119*, 20985–20992. [[CrossRef](#)]
25. Korenev, V.S.; Dorovatovskii, P.V.; Lazarenko, V.A.; Abramov, P.A.; Sokolov, M.N. Structural Features of Selenate Based {Mo 132} Keplerate Capsules. *Cryst. Eng. Comm.* **2022**, *24*, 321–329. [[CrossRef](#)]
26. Grzhegorzhevskii, K.V.; Zelenovskiy, P.S.; Koryakova, O.V.; Ostroushko, A.A. Thermal Destruction of Giant Polyoxometalate Nanoclusters: A Vibrational Spectroscopy Study. *Inorg. Chim. Acta* **2019**, *489*, 287–300. [[CrossRef](#)]
27. Ostroushko, A.A.; Tonkushina, M.O.; Safronov, A.P.; Korotaev, V.Y.; Vazhenin, V.A.; Kolosov, V.Y.; Martynova, N.A.; Kutyashev, I.B.; Bogdanov, S.G.; Pirogov, A.N.; et al. Study of the Stability of Solid Polyoxometalate Mo₇₂Fe₃₀ with a Buckyball Structure. *Russ. J. Inorg. Chem.* **2012**, *57*, 858–863. [[CrossRef](#)]
28. Tonkushina, M.O.; Grzhegorzhevskii, K.V.; Ermoshin, A.A.; Tugbaeva, A.S.; Kim, G.A.; Taniya, O.S.; Gagarin, I.D.; Ostroushko, A.A. The Electrostatic-Mediated Formation of a Coordination Complex: The Trapping and Release of an Antitumor Drug with an Anthracycline Core from {Mo 72 Fe 30}-Based Ensembles. *Chem. Sel.* **2022**, *7*, e202203684. [[CrossRef](#)]
29. Myers, H.M.; Tochon-Danguy, H.J.; Baud, C.A. IR Absorption Spectrophotometric Analysis of the Complex Formed by Tetracycline and Synthetic Hydroxyapatite. *Calcif. Tissue Int.* **1983**, *35*, 745–749. [[CrossRef](#)]
30. Mohammed, O.F.; Xiao, D.; Batista, V.S.; Nibbering, E.T.J. Excited-State Intramolecular Hydrogen Transfer (ESIHT) of 1,8-Dihydroxy-9,10-Anthraquinone (DHAQ) Characterized by Ultrafast Electronic and Vibrational Spectroscopy and Computational Modeling. *J. Phys. Chem. A* **2014**, *118*, 3090–3099. [[CrossRef](#)]
31. Bellamy, L.J. *The Infra-Red Spectra of Complex Molecules*; Springer: Dordrecht, The Netherlands, 1975; ISBN 978-94-011-6017-9.
32. Cervini, P.; Machado, L.C.M.; Ferreira, A.P.G.; Ambrozini, B.; yder Cavalheiro, T.G. Thermal Decomposition of Tetracycline and Chlortetracycline. *J. Anal. Appl. Pyrolysis* **2016**, *118*, 317–324. [[CrossRef](#)]
33. Filgueiras, A.L.; Paschoal, D.; Dos Santos, H.F.; Sant’Ana, A.C. Adsorption Study of Antibiotics on Silver Nanoparticle Surfaces by Surface-Enhanced Raman Scattering Spectroscopy. *Spectrochim. Acta Part A Mol. Biomol. Spectrosc.* **2015**, *136*, 979–985. [[CrossRef](#)] [[PubMed](#)]
34. Gražulis, S.; Daškevič, A.; Merkys, A.; Chateigner, D.; Lutterotti, L.; Quirós, M.; Serebryanaya, N.R.; Moeck, P.; Downs, R.T.; Le Bail, A. Crystallography Open Database (COD): An Open-Access Collection of Crystal Structures and Platform for World-Wide Collaboration. *Nucleic Acids Res.* **2012**, *40*, D420–D427. [[CrossRef](#)] [[PubMed](#)]
35. Krupodorova, T.A.; Barshteyn, V.Y.; Zabeida, E.F.; Pokas, E.V. Antibacterial Activity of Macromycetes Mycelia and Culture Liquid. *Microbiol. Biotechnol. Lett.* **2016**, *44*, 246–253. [[CrossRef](#)]

Disclaimer/Publisher’s Note: The statements, opinions and data contained in all publications are solely those of the individual author(s) and contributor(s) and not of MDPI and/or the editor(s). MDPI and/or the editor(s) disclaim responsibility for any injury to people or property resulting from any ideas, methods, instructions or products referred to in the content.